Estimation of Fracture Height Growth in Layered Tight/Shale Gas Reservoirs using Flowback Gas Rates and Compositions - Part II: Field Application in a Liquid-Rich Tight Gas Reservoir

C.R. Clarkson[a,*], S.M. Ghaderi[b], M.S. Kanfar[b], C.S. Iwuoha[a], P.K. Pedersen[a], M. Nightingale[a], M. Shevalier[a], and B. Mayer[a]

[a]Department of Geoscience, University of Calgary, 2500 University Drive NW Calgary, Alberta, Canada T2N 1N4
[b]Department of Chemical and Petroleum Engineering, University of Calgary, 2500 University Drive NW Calgary, Alberta, Canada T2N 1N4

**Corresponding author – Ph. (403) 220-6445, e-mail: clarksoc@ucalgary.ca*

ABSTRACT

While hydraulic fracturing is the key to unlocking the potential of unconventional low-permeability hydrocarbon resources, challenges remain in the monitoring of subsurface propagation of fractures and the determination of which geologic intervals have been contacted. This is particularly challenging for wells that are completed in multiple hydraulic fracture stages (multi-fractured horizontal wells or MFHWs) where fracture spacing may be very close and fracture geometry complex. Understanding the fracture extent is important not only for assisting with hydraulic fracture design, but also for mitigating unwanted fracture growth into non-target geologic intervals that do not contain hydrocarbons (e.g. zones with high water saturation). Popular current technologies used for hydraulic fracture surveillance include microseismic (surface and subsurface monitoring) and tiltmeter surveys. While these methods have proven useful for characterizing the extent of created hydraulic fractures, they do not necessarily lead to an understanding of what portions of the geologic section (bounding and target intervals for MFHWs, for example) are in direct hydraulic communication with the well.

A solution for establishing the extent of hydraulic fracture growth from target to bounding zones is to first obtain a fluid composition fingerprint of those intervals while drilling through them, and then compare these data with fluid compositions obtained from flowback after hydraulic fracturing. In the current work, a MFHW completed in a tight, liquid-rich (gas condensate) reservoir is used to test this novel concept. Gas samples obtained from the headspace of isojars® containing cuttings samples obtained during drilling of the MFHW well were used to geochemically fingerprint geologic intervals through which the well was drilled. The cuttings samples were collected at high frequency in the vertical, bend and lateral sections of the well over a measured depth range of 4725 ft (1440 m). A compositional marker was identified in the bend of the horizontal well above which the average methane to ethane (C_1/C_2) ratio was 15.7, versus 2.6 below it. The flowback gas compositions were observed to be intermediate (average C_1/C_2 = 7.4) between the reservoir above and below the marker, suggesting fracture height grew above the compositional marker.

In order to estimate fracture height growth from the geologic interval and flowback compositions, a compositional numerical simulation study was performed. An innovative approach was used to estimate recombined in-situ fluid compositions, on a layer-by-layer basis, by combining the cuttings gas compositional data with separator oil compositions. The resulting numerical simulation model, initialized through use of the layered fluid model and a detailed geological model developed for the subject well and offset drilling locations, was used to history match flowback rates, pressures and gas compositions. The gas compositions of the fingerprinted geologic intervals were therefore employed as a constraint on fracture height growth, estimated in the model to be 190 ft (58 m, propped height). However, because of the uncertainty in model input parameters, a stochastic approach was required to derive a range in hydraulic fracture properties.

The current study demonstrates for the first time that it is possible to constrain fracture height growth estimates from flowback data, combined with gas compositional data obtained from cuttings data, provided that the geochemical fingerprints are distinct.

Keywords: Hydraulic fracturing, Fracture height, Tight/shale gas reservoirs, Layered reservoirs, Flowback, Liquid-rich tight gas reservoir, Geochemistry

1. Introduction

Multi-fractured horizontal wells (MFHWs) have become commonplace in the development of low-permeability (tight) reservoirs, and the resulting hydraulic fracture network created during stage-by-stage stimulation treatments is critical for achieving maximum well performance (Gandossi, 2013). Therefore characterization methods that can be used to evaluate the effectiveness of hydraulic fracture networks are important for improved design of stimulation treatments. An equal, if not more important, goal of characterization, is the determination of the extent of the hydraulic fracture network spatially, including potential contact with non-target geologic intervals. One way to address these concerns, as well as improve fracture characterization for design considerations, is to provide methods that allow the portion of the geologic column that is in direct hydraulic communication with the well through the fracture network to be determined. Until now, such methods have proven elusive.

Current methods for hydraulic fracture characterization range from remote sensing to pressure-transient analysis-based techniques. These methods can be further classified by their temporal relationship to the stimulation treatment: syn- and post-stimulation (Clarkson et al., 2014). Syn-stimulation methods, which refer to characterization methods that use data collected during the stimulation treatment, include microseismic and tilmeter surveys, distributed temperature and acoustic surveys (DTS/DAS), and net pressure analysis (frac modeling). Microseismic surveys (Warpinski, 2009; van der Baan et al., 2013; Yousefzadeh et al., 2015) can be used to infer fracture location, orientation and geometry from the location of microseisms generated during hydraulic fracturing; failure mechanisms may also be inferred. Tiltmeter surveys (Wright et al., 1998; Fisher and Warpinski, 2012) may be also used to infer fracture orientation and geometry based on measured rock mass displacements, and can combined with microseismic data for improving hydraulic fracture diagnostics (Warpinski et al., 2006). DTS/DAS have proven useful for detecting sections of the horizontal lateral that have been stimulated (Cannon and Aminzadeh, 2013; Sookprasong et al., 2014; Wheaton et al., 2016), while stimulation treatment data combined with hydraulic fracture modeling can be used to interpret fracture properties such as fracture conductivity and height growth (Liu and Valko, 2015; Bai et al., 2016). None of these methods provide a direct indication of what portions of the reservoir are in direct communication with the well. Post-stimulation methods include chemical tracer surveys, pressure-transient analysis (e.g. flow/buildup welltest analysis) and rate-transient analysis of short-term (flowback) and long-term (online) production data. Chemical tracers involve doping of frac fluids with a variety of chemicals (by stage), enabling the source of inflow (success stages) to the well to be determined (Salman et al., 2014). However, native fluid properties are usually not sufficiently evaluated and considered when using this technique. Pressure-transient analysis/rate-transient analysis (PTA/RTA) techniques may be used to infer certain properties of the fracture (e.g. Barree et al., 2005) through interpretation of flow-regimes related to hydraulic fractures (e.g. bilinear, linear flow). Flowback analysis, an evolving form of RTA, has proven useful for estimation of the pore volume associated with propped and unpropped hydraulic fractures (e.g. Abbasi et al., 2014; Clarkson et al., 2014; Williams-Kovacs and Clarkson, 2016); recent studies have even included analysis of salinity and fluid chemistry data (e.g. Zolfaghari et al., 2016) to provide additional constraints on this analysis. However, these methods cannot be used to evaluate fracture height growth without additional constraints. An important additional constraint not previously considered is hydrocarbon compositions sampled from bounding and target intervals as well as the composition of flowback fluids.

In a recent study, Ghaderi and Clarkson (2016) suggested that if bounding and target interval fluids (e.g. natural gas) can be fingerprinted and are found to be geochemically distinct, then this information, combined with flowback gas compositions and rate-transient analysis of flowback rates/flowing pressures, may be used to assess the degree of fracture penetration into the bounding interval of a 2-layer system. An analytical method was developed for this purpose, and tested using numerical simulation. The initial technique however is limited to a 2-layer system, a dry gas reservoir, and assumes that the flowback signature is primarily a linear flow. With the current focus of unconventional reservoir development on liquid-rich plays, and with the possibility of more complex reservoir behavior, more sophisticated methods such as compositional numerical simulation may be required to interpret fracture height growth using flowback data.

Kanfar and Clarkson (2016) recently demonstrated a workflow that combined compositional numerical simulation (using a triple porosity framework for modeling the hydraulic fracture network) with stochastic methods to enable flowback and online production data to be interpreted for fracture and reservoir properties associated with a liquid-rich tight gas reservoir. However, fracture height was assumed to be constrained to the height of the target interval. The current work expands the use of the Kanfar and Clarkson (2016) approach for flowback analysis to include estimation of fracture height growth by adding reservoir/flowback fluid compositions as a constraint.

The objective of this study was to develop a combined geochemical and modeling approach that enables estimation of fracture height growth in reservoirs where fluid chemistries vary vertically. The herein presented case study illustrates the use of gas compositions collected while drilling, as well as flowback fluid compositions, to constrain

fracture height estimation obtained from compositional numerical simulation. Gas cuttings samples, collected while drilling and placed in isojars®, were used to derive gas sample fingerprinting at a high resolution in the vertical, bend and lateral sections of a well completed in a liquid-rich tight gas reservoir. These data in turn allowed gas compositions at various intervals within the zone containing the well to be distinguished. After hydraulic fracture stimulation of the subject well heel stages, the flowback fluids were sampled and gas compositions determined to allow for comparison with those obtained while drilling. A detailed geologic model, constructed for the development area containing the subject well, as well as the new gas compositional data, provided the framework for a compositional numerical simulation model used to predict fracture height growth. In the following, the methods for field data collection, geologic model construction, and numerical model setup and implementation are first provided, followed by a presentation of the results of gas fingerprinting and numerical modeling.

2. Methods

The subject horizontal well (located in Western Canada) was drilled to a measured-depth of 18110 ft (5520 m) with a kickoff point of 9905 ft (3020 m). The lateral section was directionally drilled from 10545 ft (3214 m) to TD. An oil based mud was used to drill to the intermediate casing point, while a water based mud was used to drill out the lateral section. A toe-up configuration was used for the lateral (**Fig. 1**). During the openhole completion, mechanical difficulties resulted in the implementation of only 9 of the planned 28 stages in the heel of the well. For each stage, approximately 2000 bbls of water and 5 MMscf of nitrogen were injected at around 9000 psi (average formation fracture pressure estimated to be 7,000 psi); approximately 240 tonnes of 40/70 mesh size sand was used for proppant. Additional details of the well drilling and completion are withheld to preserve operator confidentiality.

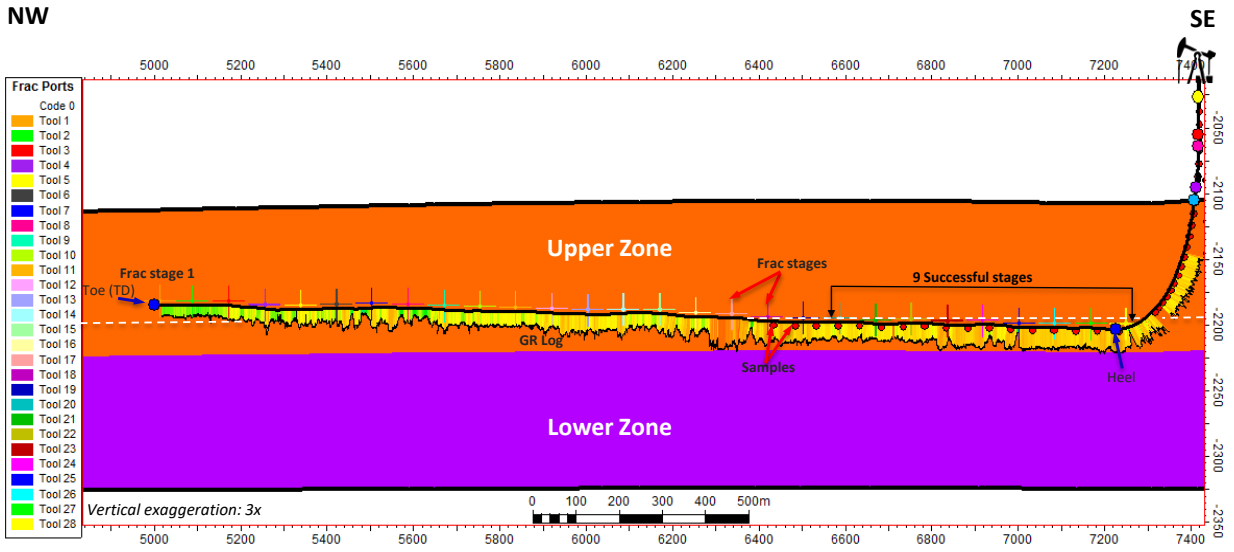

Fig. 1. Cross-section created in Petrel™ illustrating horizontal lateral trajectory with respect to upper and lower zones identified during geologic modeling, location of 9 successful hydraulic fracturing stages, and location of the cuttings samples analyzed for gas composition. Also projected are the initial designed hydraulic fracturing stages (not yet implemented). A gamma ray log is provided to illustrate lithology/reservoir quality variation along the lateral. Finally, a "compositional marker" (white dashed line) is shown where a distinct shift in C_1/C_2 ratio was identified from cuttings analysis (see Section 3.1 for discussion). Note: Cross section depth scale is in true vertical depth subsea (TVDSS) with 3.28 ft = 1m.

2.1. Field sample and data collection

A total of 56 cuttings samples collected in isojars® in the vertical, bend and lateral sections of the subject well were taken over a measured-depth range of approximately 8612 – 13337 ft (2625 – 4065 m). The sample frequency was every 82 ft (25 m) in the vertical section of the well, every 33 ft (10 m) in the bend and every 164 ft (50 m) in the lateral section. 250 mL of cutting samples were collected and stored in water in isojars®, making a total volume of 500 mL, which contained a biocide to prevent microbial degradation of the methane and ethane. These samples were

allowed to stand for 2 weeks to permit a complete degassing of the cuttings. The headspace gas of the isojars® was sampled and analyzed using a gas chromatrograph with a flame ionization detector for determining methane and ethane concentrations and thermoconductivity detector for carbon dioxide and nitrogen concentrations at the University of Calgary's Applied Geochemistry group (AGg) laboratory. Although there is some methane and ethane dissolved in the water leg of the isojar®, the ratio of methane to ethane in the headspace gas is constant for each analyzed sample.

For flowback fluid sampling, fluid from the separator was first flowed for 60 seconds to flush out residual fluids from the lines before the sample was taken. Samples were collected after 100 m^3 of fluid flowback and fifteen fluid samples were collected. These samples were collected in 1 L HPDE Nalgene® bottles, filled to the top leaving no head space. For flowback gas sampling, the gas was allowed to flow for 30-60 seconds to flush out stale gas from the separator lines. Three gas samples were extracted for gas chromatographic analysis at early, middle and late times during the flowback process. All fluid and gas samples were shipped to the AGg for composition and isotopic analysis.

Flowback gas and water samples were analyzed for chemical and isotopic compositions. As these data provide an excellent means to track the evolution of the frac/formation fluid admixtures, they will be incorporated into future studies of fracture propagation.

During the flowback process, gas, condensate (or oil), water and casing pressures were monitored at 30 minute intervals. These data, along with flowback gas compositions, served as the basis of the numerical model history-matching discussed below. Salinity of the flowback fluids was also measured periodically. Finally, because an N_2 foam frac was performed, the relative percentage of N_2 in the flowback gas was also monitored.

Well logs were available for the subject well and offset vertical and horizontal wells. The principal logs used for construction of the study area petrophysical model included: gamma ray, resistivity (shallow, medium, deep), neutron porosity, bulk density, density porosity. For the study well, a deviation survey, strip log, caliper, logging while drilling (LWD) gamma ray, neutron, density and resistivity logs were available.

One well in the study area, adjacent to the subject well, contained a core for which detailed core analysis was performed (Ghanizadeh et al. 2015a,b). These data, used for log calibration, included: helium porosity, pressure-decay profile permeability, pulse-decay permeability, micro hardness (for mechanical properties), grain density and bulk density.

2.2. Geologic model construction

A stochastic geologic model was constructed using the Petrel™ software. The modeled area includes the study well, plus 8 offset wells (vertical and horizontal), and covers 29 square-miles (75 km^2). The workflow used in constructing the geologic model is summarized in **Fig. 2**. A brief description of some of these steps is provided below.

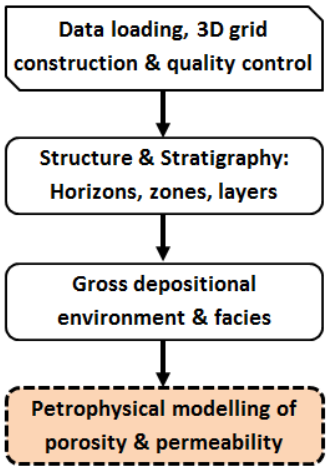

Fig. 2. Workflow used in geologic model construction.

3D Grid Construction. The 3D grid was designed to allow the transfer of vertical and horizontal heterogeneities to the numerical simulator. The 3D grid properties are as follows:

- Active 3D grid cells: 2.1 million
- Cell dimensions: 75m x 75m x 1.6m

- SW Structural dip: consistent with regional understanding of the geological formation
- Grid orientation: -045^0 : to be consistent with paleo-shelf edge orientation, as well as regional depositional trends
- Geological layers: 137

The grid was oriented to be approximately orthogonal to dip of the upper zone structure, and parallel to horizontal well trajectories.

Structural and Stratigraphic Modeling. All horizons, including the upper and lower horizons (Fig. 1), were created using the "Make Horizon" process in Petrel. The surface of the upper horizon was created using well tops from all 9 wells in the study area. The basal unit underlying the lower horizon was mapped using 3 offset vertical wells. No faults or fractures were considered in the static modeling. A two-step process was used for stratigraphic modeling: reservoir zone mapping and layering. For the former, the "Make Horizon" process in Petrel was used to define the upper and lower zones in the model – an example cross-section illustrating the location of the cored well and study well is provided in **Fig. 3**. For the latter, a total of 137 geologic layers (71 for upper zone and 66 for the lower zone) were defined with an average thickness (cell height) of 5.25 ft (1.6m), which is considered sufficient to capture vertical heterogeneities. The number of layers assigned to each zone was determined by the average gross thickness of each zone calculated from vertical wells in the study area.

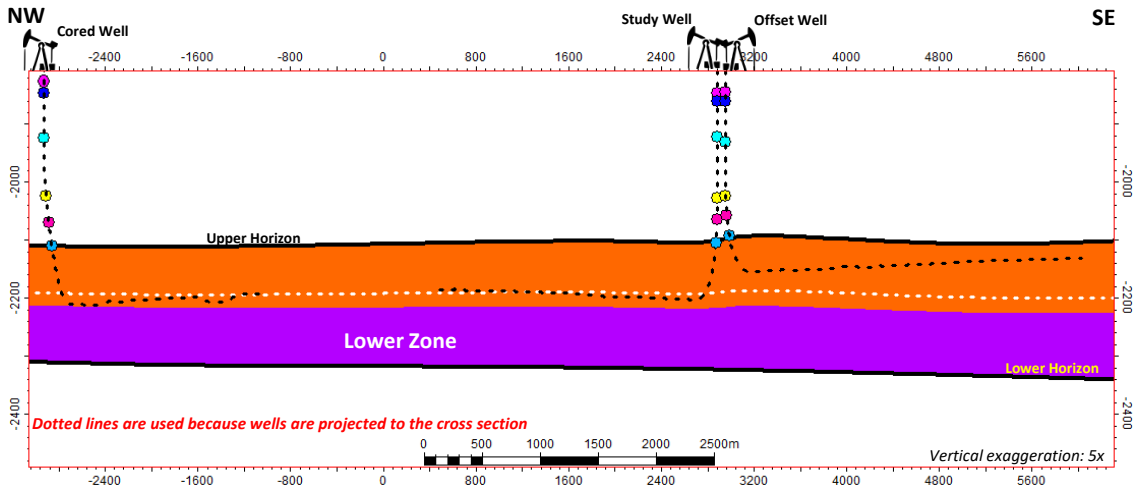

Fig. 3. Cross section through the core of the study area showing location of horizons and zones within the target formation. Well trajectories are shown with black dashed lines. A "compositional marker" (white dashed line) is also shown where a distinct shift in C_1/C_2 ratios was identified from cuttings analysis (see Section 3.1 for discussion).

Facies Modeling. This stage in the workflow commenced with identifying the gross depositional environments (GDEs) in the geological formation under study. A generalized nomenclature (modified from Kuppe et al., 2012) was implemented in order to capture field-scale depositional variations in the upper and lower zones. The following GDEs were assigned:

- Upper zone: proximal shelf environment (PSE)
- Lower zone: distal shelf environment (DSE)

A multi-step process was then used to populate facies in the GDEs. The steps included lithofacies recognition and distribution in 3D space. Lithologies intersected by wells (predominantly sands, silts and shales) were retrieved from strip logs or core logs for several wells in the study area. Two approaches for defining petrofacies were investigated to capture geological heterogeneities: petrofacies defined by gamma ray (GR) cutoffs only, and petrofacies defined using a combination of GR and resistivity (RES) logs (Nieto et al., 2009).

The latter approach, however, resulted in undefined facies log sections in the wells that did not meet Nieto et al.'s (2009) criteria. On the contrary, the GR-only approach resulted in clear distinction of sands, silts and shales in all the

GDEs (PSE and DSE) and was therefore used to generate the facies log. The cut-off criteria used in the GR-only approach were:

- Sands: GR<60 API
- Silts: 60<=GR<=115 API
- Shale: GR>115 API

For lithofacies 3D population, the following steps were taken:

- The lithofacies defined at the wells were scaled-up to the 3D grid using the "Most of" algorithm in Petrel™
- Facies proportions were estimated from the lithofacies logs at the wells.
- Truncated Gaussian distribution was used in the "Facies Modeling" process in Petrel™ to distribute the lithofacies in 3D in the GDEs.

The facies model was quality controlled to ensure that modeled facies proportion was consistent with the facies proportion seen at the wells in the upper and lower zones. **Fig. 4** illustrates the results of facies modeling.

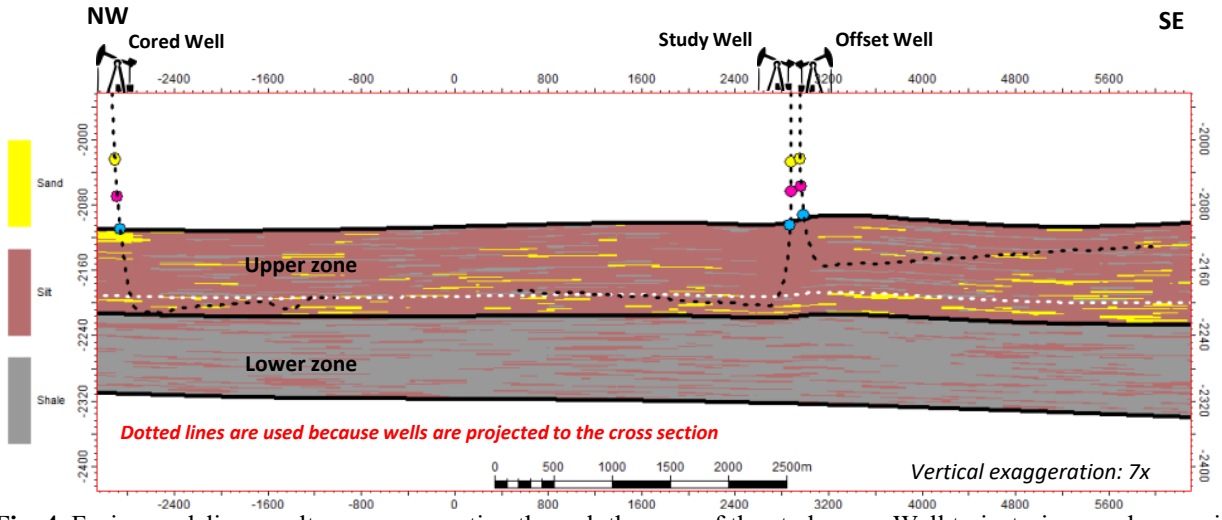

Fig. 4. Facies modeling results – a cross-section through the core of the study area. Well trajectories are shown with black dashed lines. A "compositional marker" (white dashed line) is also shown where a distinct shift in C_1/C_2 ratios was identified from cuttings analysis (see Section 3.1 for discussion).

Petrophysical Modeling. Two petrophysical properties, porosity and permeability, were estimated using core-calibrated log data. Core plug porosity estimates using a helium pycnometer were available from the offset cored well (Ghanizadeh et al. 2015a). Log-derived porosity, estimated from the bulk density log using a matrix density of 2.71 g/cm (in line with core measurements), is in reasonable agreement with the core porosity values (**Fig. 5**). Scale-up of the log-derived porosity values to the 3D grid was achieved using an arithmetic average method in Petrel™. The Sequential Gaussian Simulation algorithm was used in the Petrel "Petrophysical Modeling" process to distribute porosities throughout the study area. **Fig. 6** illustrates the resulting porosity distribution in each zone in the core of the study area. It is evident that the upper zone has relatively better reservoir quality than the lower zone.

For permeability modeling, profile permeability values (corrected to in-situ stress) obtained for sections of slabbed core in the offset cored well (see Fig. 6 for location relative to study well) were scaled-up to log scale using the approach of Clarkson et al. (2012) and cross-plotted with log-derived porosities (**Fig. 7a**). In addition, pulse-decay permeability values obtained on core plugs subjected to in-situ stress are also shown (**Fig. 7b**). A weak correlation between permeability and porosity is exhibited likely due to 1) difference of log and core scales and 2) the primary control on permeability being pore throat size. As a result, permeability prediction from logs is poor, as evidenced from comparison of log and core-derived permeabilities as a function of depth displayed in **Fig. 5**. Permeability estimated through petrophysical modeling was used as the matrix permeability estimate in simulation modeling.

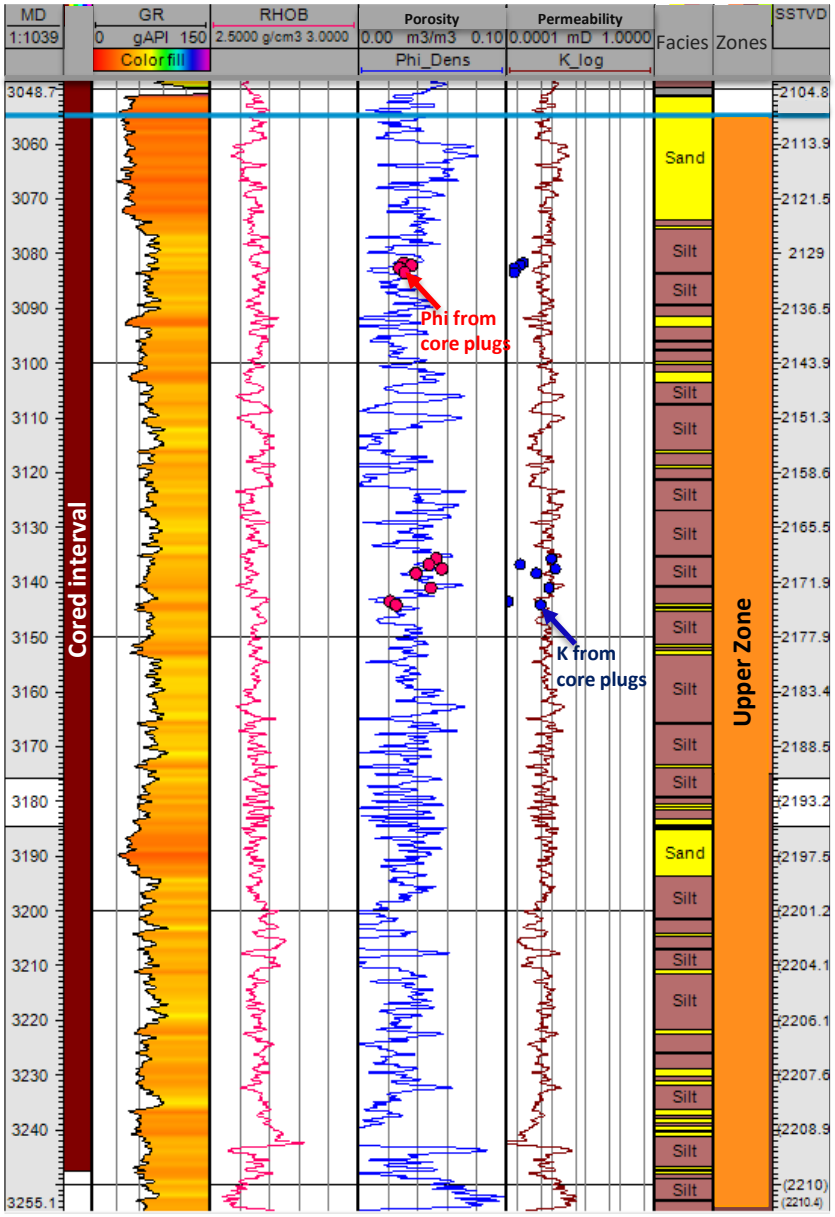

Fig. 5. Comparison of log-derived porosity and permeability versus core data (tracks 4-5, respectively). The horizontal blue line depicts the top of the upper zone. A core-to-log depth shift was applied.

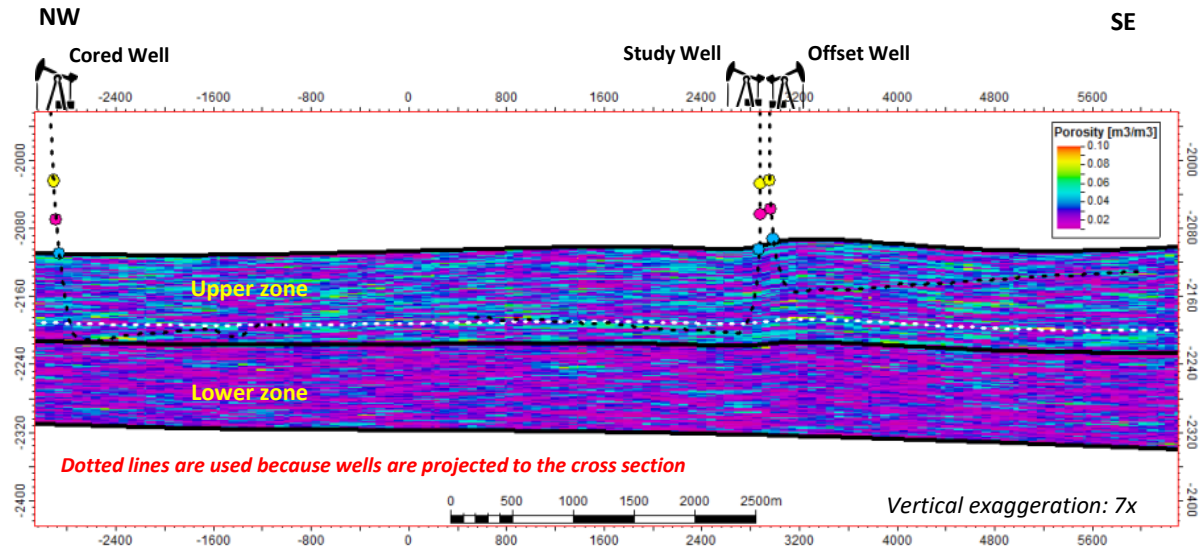

Fig. 6. Porosity modeling through core of study area. Well trajectories are shown with black dashed lines. A "compositional marker" (white dashed line) is also shown where a distinct shift in C_1/C_2 ratios was identified from cuttings analysis (see Section 3.1 for discussion).

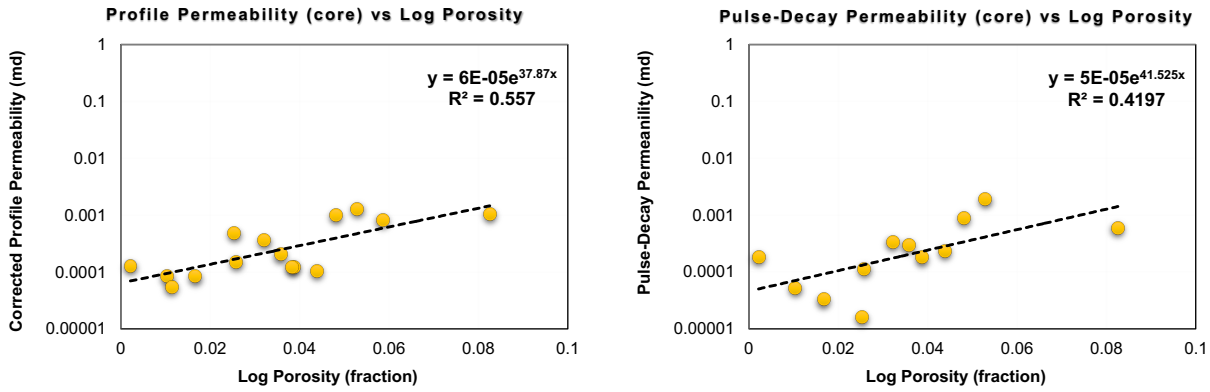

Fig. 7. (a) Cross plot of profile (probe) permeability and log-derived porosity; (b) Cross plot of pulse-decay permeability and log-derived porosity. Core data from Ghanizadeh et al. (2015a).

2.3. Reservoir simulation modeling

A numerical simulation model was constructed in Eclipse 300™ in order to capture vertical and lateral heterogeneity in porosity, permeability and gas compositions obtained from cuttings samples. Although a larger area was used in the construction of the geomodel discussed above to allow the capture of offset well data (core and log), a small portion of the model is sufficient for simulation history-matching. Because the history-match was only performed over the flowback period (around 9 days), the distance of investigation by pressure and saturation is limited to a reservoir region in the vicinity of the hydraulic fracture (HF); therefore, only a small area of the geomodel was utilized.

Model Gridding and Property Modeling. A symmetric model (quarter fracture model) in the vicinity of one stage of the HF plane was created. This planar HF is exposed to the reservoir from one side. **Table 1** provides a summary of grid properties obtained from a geomodel realization, including the high, medium and low values of porosity and permeability in the simulation grid. **Fig. 8** graphically illustrates porosity and permeability assigned to the grid adjacent to the HF plane. The porosity values were up-scaled from the finely gridded geomodel while the permeability values were obtained from the porosity-permeability relationship.

As mentioned, the HF plane is embedded within the main simulation grid and coincides with *x* grid face direction. Local grid refinement (LGR) is used to incorporate the hydraulic fracture into the reservoir model. In addition, LGR is used to refine grid blocks around the fracture plane. Specifically, logarithmic-gridding is applied in which very small blocks are placed in the vicinity of the fracture. These grid blocks are logarithmically proportional to each other in size with larger grid blocks away from the fracture plane. Fine gridding is essential to model large pressure changes near fractures – a characteristic of tight/shale reservoirs. Moreover, logarithmic spacing preserves the total number of simulation grids at a manageable level.

Two important assumptions were made in the construction of the simulation model: 1) the flow system exhibits dual porosity behavior, with reservoir and HF acting as the two interacting systems; 2) the HF plane consists of two different "un-propped" and "propped" segments, with the latter associated with better flow characteristics (in terms of permeability and porosity). **Fig. 9** displays the fracture embedded within the model grid, and multiple applications of logarithmic refinement to obtain propped and un-propped zones within the fracture plane.

Table 1
Properties assigned to grid.

Property	Value	Unit
Grid top	6920	ft
Nx, Ny, Nz	10, 1, 30	[-]
Dx, Dy, Dz	160, 165, 24	ft
K_m (min), K_m (med), K_m (max)	100, 700, 2540	nd
Φ_m (min), Φ_m (med), Φ_m (max)	0.0036, 0.0287, 0.0821	fraction
Reservoir temperature	195.8	ºF
Reservoir initial pressure	5350	psia
Initial water saturation	0.31	fraction

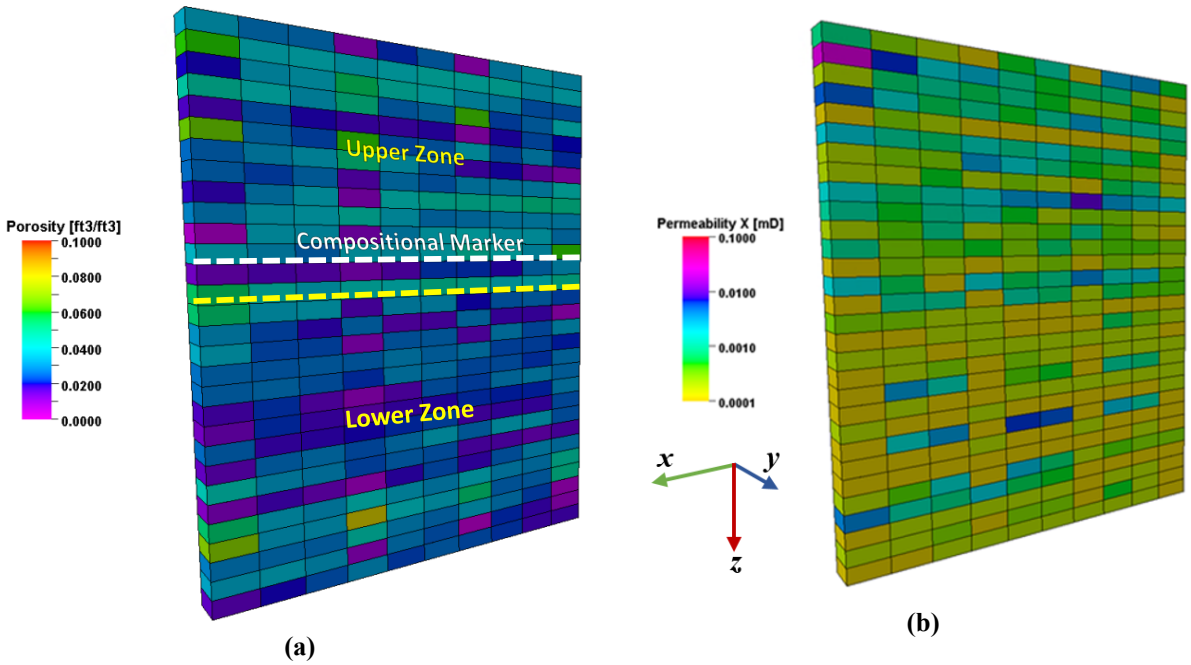

Fig. 8. (a) Matrix porosity and (b) matrix permeability assigned to the grid adjacent to the hydraulic fracture. Layers 1 to 14 represent the upper zone, and 15 to 30 represent the lower zone. In (a), the white dashed line corresponds to a "compositional marker" where a distinct shift in C_1/C_2 ratios was identified from cuttings analysis (see Section 3.1 for discussion). The yellow dashed line depicts the boundary between upper and lower zones.

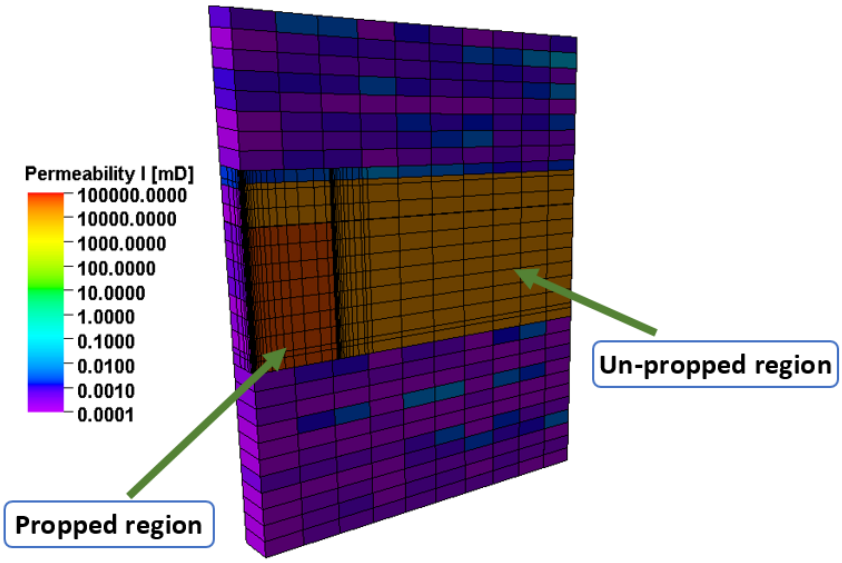

Fig. 9. Local grid refinement, with logarithmic spacing, is used to create the hydraulic fracture plane within the model grid. The hydraulic fracture is further differentiated into two regions: propped and un-propped, with different properties (i.e., permeability and porosity). Note that the fracture height covers portions of the upper and lower zone.

Fluid Property Modeling. In this work, an innovative approach for estimating the in-situ fluid composition of this liquids-rich reservoir as a function of depth was employed, as illustrated in **Fig. 10**. Gas compositions obtained from cuttings samples in isojars® were recombined with oil compositions obtained from the separator to calculate the re-combined in-situ fluid composition as a function of depth. Recombination was performed based on the component-based material balance as outlined by McCain (1990).

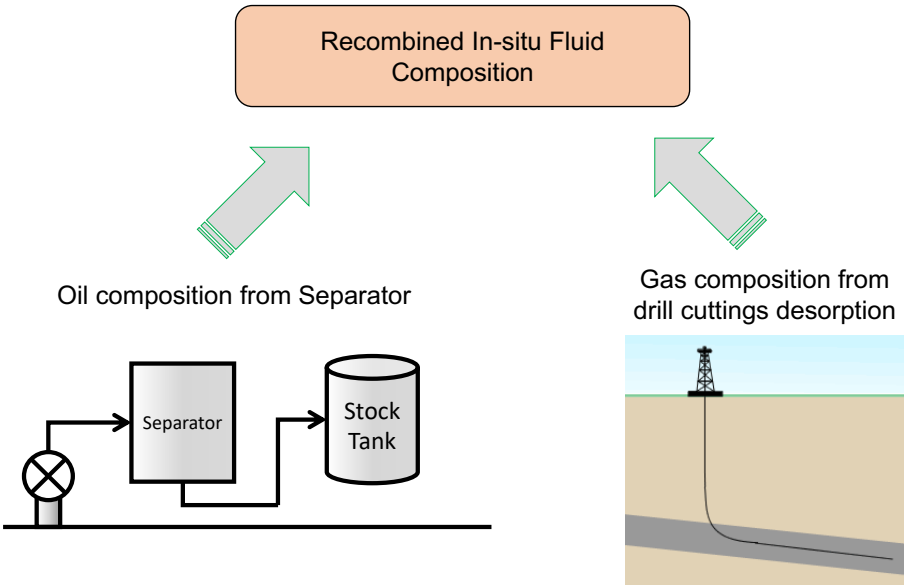

Fig. 10. Illustration of the use of cuttings gas sample compositions and surface separator oil compositions to estimate recombined in-situ fluid compositions as a function of depth in the model.

As with petrophysical properties discussed in the previous section, gas compositions from cuttings were first assigned to the geological grid. **Table 2** contains the C_1 and C_2 concentrations and ratios, obtained from cuttings

samples, assigned to the vertical gridblocks in the simulation model. The recombined fluid compositions are averaged in the vertical direction using sample data residing within each layer. For averaging, the compositions which are located at the measured depth of the layer top and bottom are used. However, composition is assumed to be invariant in the horizontal direction of each layer.

Table 2
C_1 and C_2 concentrations and their ratio (C_1/C_2).

Z Block	C1 (%)	C2 (%)	C1/C2	Zone
1	71.32	5.17	13.79	
2	73.91	3.81	19.40	
3	72.08	4.77	15.11	
4	67.17	7.34	9.15	Upper
5	74.89	3.29	22.76	
6	62.00	10.05	6.17	
7	61.36	10.39	5.91	
8	62.58	9.75	6.42	
9	64.98	8.49	7.65	
10	67.07	7.39	9.08	
11	69.10	6.33	10.92	
12	71.51	5.07	14.10	Compositional Marker
13	44.98	18.98	2.37	
14	45.79	18.56	2.47	
15 - 30	56.78	12.80	4.44	Lower

At initial reservoir conditions, the in-situ fluid is gas (gas condensate system). **Fig. 11** presents the phase envelope of the richest and leanest fluids in **Table 2**. It is important to note that the phase envelopes and in-situ fluid properties will differ layer-by-layer in the model because of the differing cuttings gas compositions; however the depicted phase envelopes in **Fig. 11** indicate the range of variability that would be encountered during production. In other words, all other compositions will have a phase envelope lying between these two.

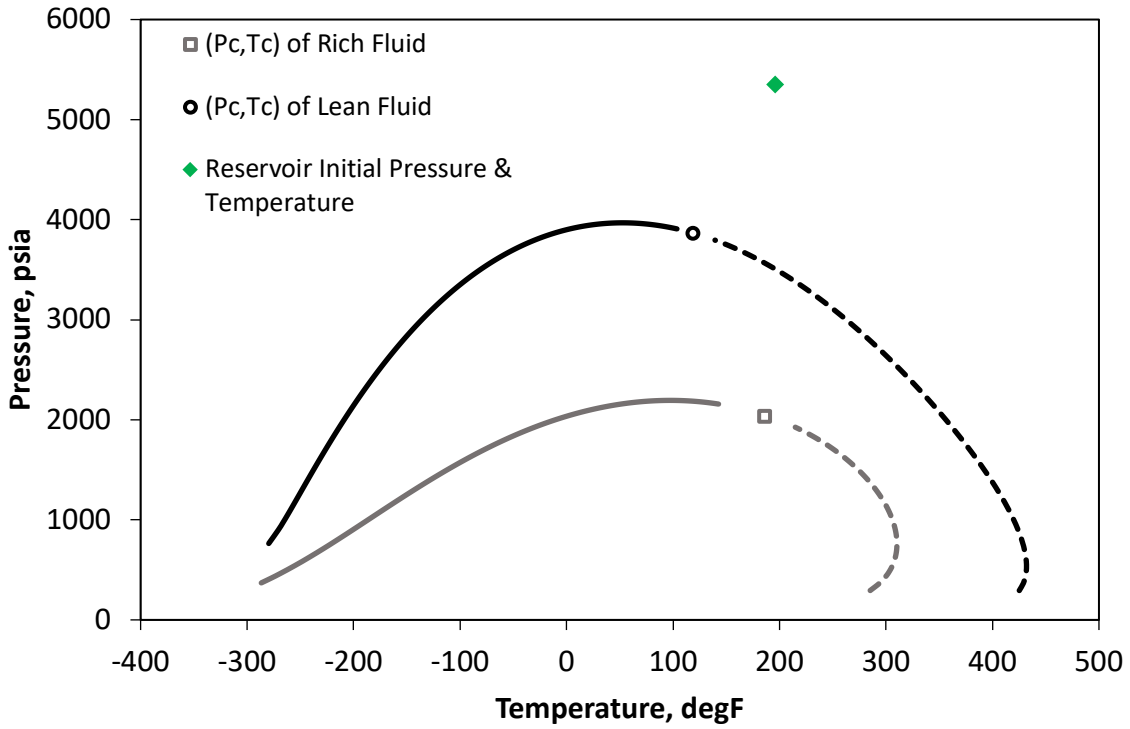

Fig. 11. Phase envelopes associated with the richest and the leanest fluids (layers 13 & 5, respectively) in the system. Reservoir initial conditions are also depicted.

Fracture Property Modelling and Model Initialization. Permeability and porosity of the fracture is assumed to be homogenous, but assigned different values in propped and un-propped regions. Fracture (half) width is also fixed at a value equal to 0.03 ft with 100% porosity (as starting point) for the un-propped region; porosity of the propped region is used as a tuning parameter during history matching. The porosity of the propped region is used, combined with the mass of injected proppant, to calculate initial propped fracture volume. As foamy nitrogen was used as fracturing agent, N_2 must be included in the fluid model. At time zero, the fracture is assumed to be filled with water and nitrogen. For matrix fluid composition, the values provided in Table 2 were used.

Relative Permeability and Stress-Dependent Permeability Modelling. Relative permeability and capillary pressure curves were generated using the equations of Brooks and Corey (1964). Different sets of relative permeability curves are used for the matrix and two regions of the hydraulic fractures. However, capillary pressure is only applied to the matrix and neglected in the fracture plane. Further, because pressure decline within the fracture is large during the flowback and subsequent production periods, permeability and capillary pressure are usually pressure dependent (Hou et al., 2014). This dependency of permeability on pressure is modelled using Pedrosa's equation (Pedrosa, 1986) and neglected for capillary pressure.

Stochastic Modelling Approach. The history-match of flowback production data was conducted through sensitivity analysis of important uncertain parameters, including hydraulic fracture and matrix properties, relative permeability data etc. The well constraint used is flowing bottom-hole pressure (BHP). Because the field-measured data are provided as wellhead pressures, Beggs and Brill's correlation (1973) is used to derive the corresponding BHP values.

Table 3 presents a summary of history matching parameters and the bounding limits associated with each parameter.

To explore all combinations of these parameters, and in order to minimize the mismatch between the observed production data for three phases and the simulation results (objective function), a multi-objective optimization (MOO) algorithm is required. For this, the fast non-dominant sorting genetic algorithm (NSGA-II) was used.

Table 3
The history matching parameters and their range.

Matching Parameters	Lower Bound	Upper Bound
Factor 1: log10 of Pedrosa coefficient (Propped Fracture)	-6	-2
Factor 2: log10 of Pedrosa coefficient (Unpropped Fracture)	-6	-2
Factor 3: xf, ft (Propped fracture)	100	700
Factor 4: log10 of Permeability (Unpropped Fracture)	2	5
Factor 5: log10 of Permeability (Propped Fracture)	2	5
Factor 6: Sw (Matrix)	0.1	0.5
Factor 7: Swc (Matrix)	0	0.5
Factor 8: Sor (Matrix)	0	0.3
Factor 9: Sgc (Matrix)	0	0.3
Factor 10: krwiro	0.5	1
Factor 11: krogcg	0.5	1
Factor 12: krgcl	0.5	1
Factor 13: Ratio of unpropped fracture volume beyond fracture tip to total unpropped volume	0.1	0.9
Factor 14: Threshold of Capillary Pressure	10	300
Factor 15: Slope of Capillary Pressure Curve	0.5	2
Factor 16: Nw (Matrix)	1	10
Factor 17: Now (Matrix)	1	10
Factor 18: Nog (Matrix)	1	10
Factor 19: Ng (Matrix)	1	10
Factor 20: Nw (Fracture)	1	2
Factor 21: Now (Fracture)	1	2
Factor 22: Nog (Fracture)	1	2
Factor 23: Ng (Fracture)	1	2
Factor 24: FORCH Coefficient	0	50
Factor 25: Porosity (Propped Fracture)	0.15	0.48
Factor 26: log10 fracture compressibility (Unpropped)	-6	-3
Factor 27: log10 fracture compressibility (Propped)	-6	-3

The application of NSGA-II has several advantages. One of the main advantages is that it does not require pre-determined weighting of objectives. For example, gas, due to its high mobility, is the dominant producing fluid in the studied gas condensate system; under such conditions, the gas production match would need to be assigned a higher weighting factor in the objective function. The exact weight necessary to find an optimum cannot be determined without extensively investigating the effects of different weights on the goodness of fit, which is computationally expensive. However, using the multi-objective optimization of NSGA-II, no weights are necessary because each phase misfit is treated as a separate objective function. With this approach, the weights only need to be determined after optimization is completed by choosing the best solution from the Pareto optimum front. Another advantage of NSGA-II is that it is an evolutionary-based algorithm and not gradient-based. This characteristic enables NSGA-II to theoretically find the global optimum even if the function is non-convex. This is a big advantage when solving the current problem because the objective function used herein cannot be determined analytically, and therefore convexity cannot be proven without prohibitive search. Finally, the NSGA-II is suitable for objectives that are conflicting, which may arise from noisy data (Kanfar and Clarkson, 2016). For details about NSGA-II and its application to history matching, the reader is referred to the work of Kanfar and Clarkson (2016).

In this work, NSGA-II is used to find a Pareto optimum front. After the Pareto front is obtained, solutions are filtered following the same approach of Kanfar and Clarkson (2016) to arrive at a final solution. The NSGA-II is setup

to run 50 generations, each consisting of a population of 100 – a total of 5000 simulation runs. After each generation, solutions (parents) are selected based on binary tournament selection, and then new solutions (children) are produced by adapting a continuous cross-over. In addition to this, the algorithm is allowed to explore the solution domain by imposing a 15% mutation rate. Only solutions with a low misfit (high fitness) are chosen to form the next generation while other solutions are discarded. The fitness is determined using the objective function. Details of the NSGA-II setup are summarized in **Table 4**.

Table 4
Genetic algorithm setup and objective function.

Number of Generations	50
Population Size	100
Selection Method	Binary Tournament
Cross-over Method	Continuous Cross-over
Mutation Rate	15%
Objective Function	$\sum_{i=1}^{n} \frac{\left(Q_i^{obs} - Q_i^{sim}\right)^2}{n}$

As can be seen from Table 4, history match quality was quantified using the least squares method; minimization of the square root of residuals (the difference between observed and simulated cumulative production) is sought. In order to rank the uncertain parameters in terms of their impact on the variation of each objective function (3 objective functions, one for each phase), sensitivity analysis of proxy models is conducted. For proxy model development, the response surface method (RSM) is utilized to generate quadratic surfaces (polynomials). The proxy models are then used to generate a Tornado plot, which represents the sensitivity analysis graphically.

Fracture Height Estimation. In order to obtain a reasonable estimate of fracture height, the following constraints are recommended: 1) initial propped fracture volume, obtained as explained above; 2) composition of in-situ fluid versus depth through target formation and 3) flowback fluid compositions. For 1), the initial volume of the propped fracture is estimated in advance using data obtained from the frac job report. Accordingly, with known fracture width (which is assigned a fixed value), the only remaining unknowns are fracture length and height. If one of the parameters is adjusted, the others are readily determined through material balance calculations ($frc.height = \frac{frac.Volume}{fac.\ length \times frac.\ width}$). For 2) and 3), if zones within the geologic formation containing the well have distinct compositional fingerprints, then the amount of fracture plane exposed to these zones will affect the producing condensate-gas ratio (CGR) values and the flowback fluid compositions. Therefore, with known initial geologic interval and flowback compositions, the fracture height can be adjusted until the simulated producing composition matches the measured flowback composition. **Fig. 12** provides a flowchart summarizing the proposed workflow for fracture height estimation used in this study.

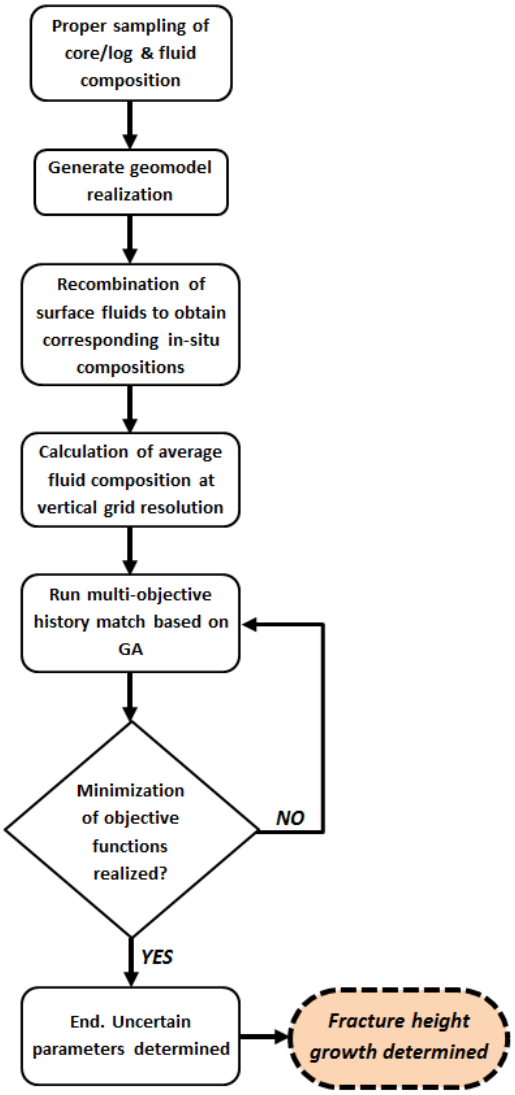

Fig. 12. Flowchart of the proposed workflow for fracture height estimation used in this study.

3. Results

In this section, the results of cuttings and flowback gas composition analysis will first be presented. Then, the results of stochastic simulation history-matching, and specifically fracture height-growth estimation, are presented and discussed.

3.1. Vertical distribution of gas composition in the formation

To assess the distribution of gas compositions obtained from cuttings, C_1/C_2 ratios were plotted for all analyzed cuttings samples (**Fig. 13**). The vertical, bend and lateral sections of the well are approximately located by sample, as is the target formation. A clustering of C_1/C_2 ratios was observed, with gas compositions associated with Cluster 2 being richer in C_1 (average C_1/C_2 ratio = 15.7) than Cluster 3 (average C_1/C_2 ratio = 2.6) or Cluster 1 (average C_1/C_2 ratio = 6.6). These gas compositions are plotted along with the well trajectory in **Fig. 14**. For reference, the locations of successful fracture stimulation stages are also provided.

The compositional distinction observed between Cluster 2 and Cluster 3, located in the upper zone, were used to define a "compositional marker", which is depicted in Figs. 1, 3, 4, 6 and 8.

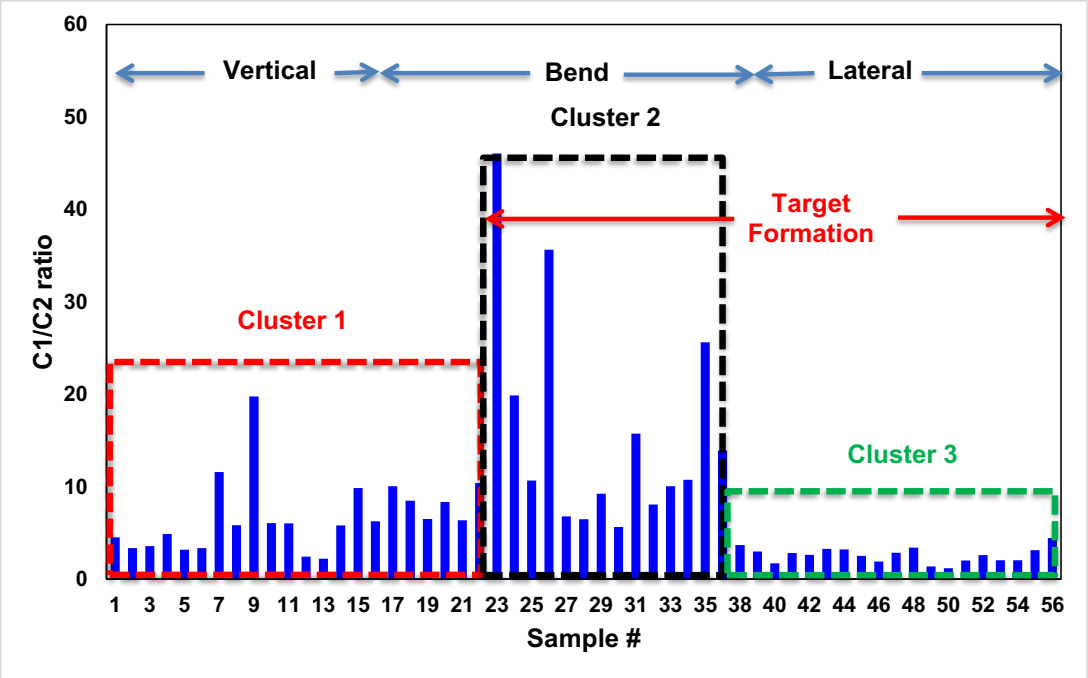

Fig. 13. C_1/C_2 ratios for all cuttings samples.

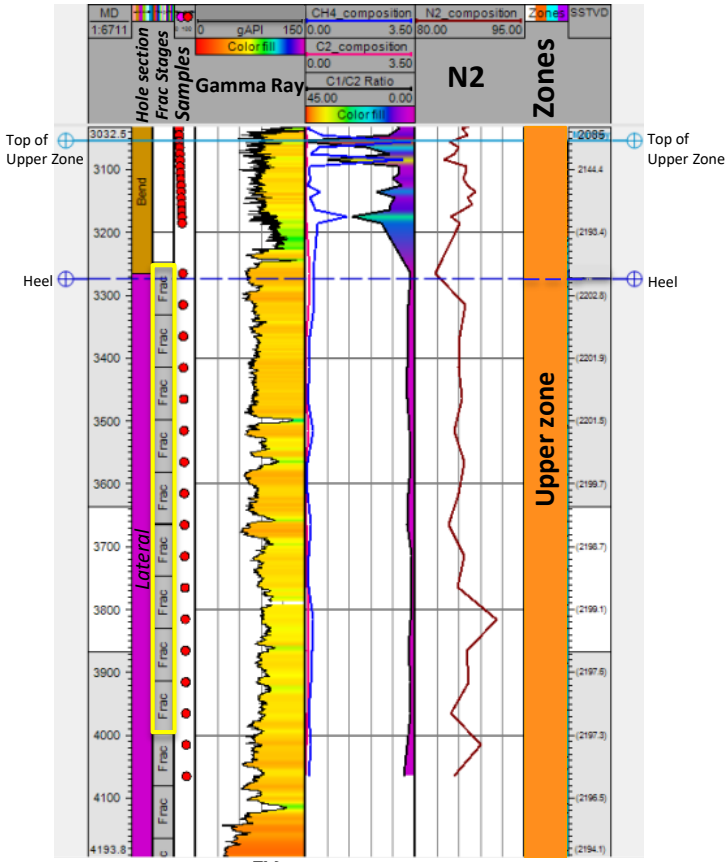

Fig. 14. Measured-depth profile created in Petrel™ illustrating gas compositional variation (C_1/C_2) by zone. Note that the higher C_1/C_2 ratios appear in the heel of the well. For reference, the successful fracturing stages are highlighted (yellow box).

3.2. *Flowback fluid compositions*

As noted in the "Methods" section, flowback gas compositions were also measured during early, middle, and late stages of flowback. A comparison between flowback gas compositions and cuttings sample gas compositions is provided in **Fig. 15**. From this comparison, it is evident that the flowback gas compositions are intermediate (average C_1/C_2 ratio = 7.4) between Cluster 3 (average C_1/C_2 ratio = 2.6) and Cluster 2 (average C_1/C_2 ratio = 15.7), which suggests that the fracture has propagated above the compositional marker (boundary between Cluster 3 and 2). This information is used as a constraint on fracture height growth, as discussed further below.

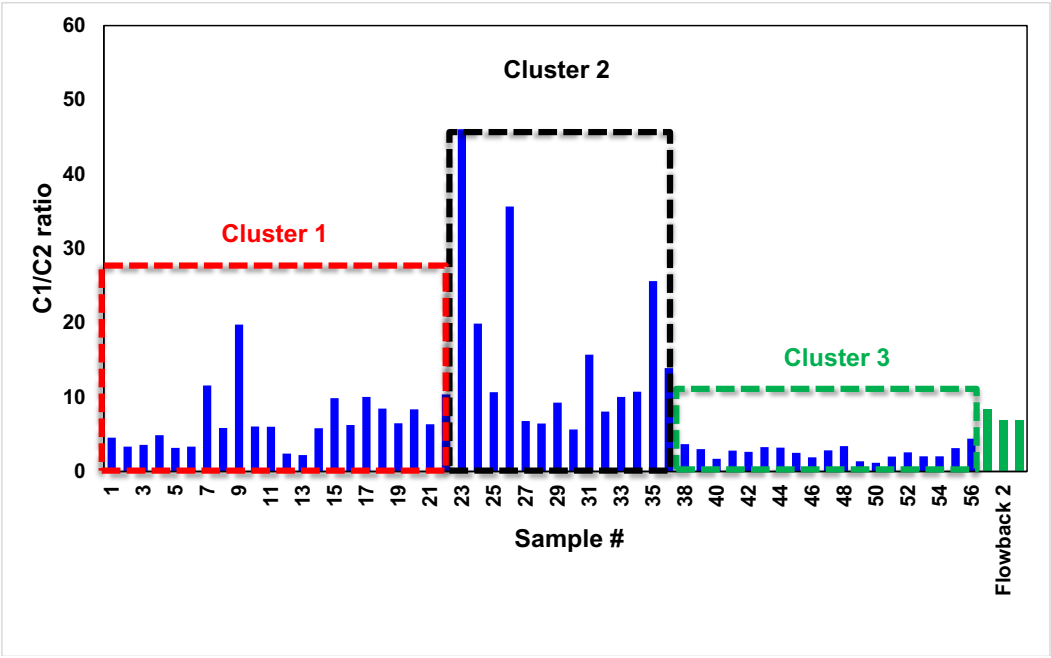

Fig. 15. Comparison of C_1/C_2 ratios for cuttings samples (blue bars) and flowback samples (green bars).

3.3. *History-match results and fracture height estimation*

Fig. 16 provides the results of the best history-match obtained through optimization, while **Table 5** provides the final values of parameters adjusted during the matching exercise. BHP (Fig. 16a), which was used as model input during the flowback period, declines steeply (decline rate of approximately 370 psi/day), meaning that flowing pressure drops below dewpoint pressure (varies by layer, but in the range of 3500-2000 psi) near the end of the flowback period. A good match for gas cumulative production through the entire flowback period was obtained (Fig. 16b). The match of condensate (Fig. 16c) and water (Fig. 16d) is also reasonable. The condensate-gas-ratio (CGR) match is mostly dependent on the fracture height exposed to the layers of variable composition, while the water-cut is heavily dependent on both the fracture surface area and capillary pressure values.

While **Table 5** provides final values for all optimized model parameters, **Table 6** provides only the values obtained for the hydraulic fracture. It can be seen that the propped fracture height (constrained by layer and flowback compositions) is estimated to be around 190 ft – fracture growth above the compositional marker (71 ft above the well; 118 ft below it) is predicted. As mentioned previously, fracture exposure to different layers of varying compositions affects the composition of the outflow stream and therefore the produced CGR. The final match results suggest that the fractures extended downward (towards lower C_1/C_2 ratios) more than upward (direction of higher C_1/C_2 ratios).

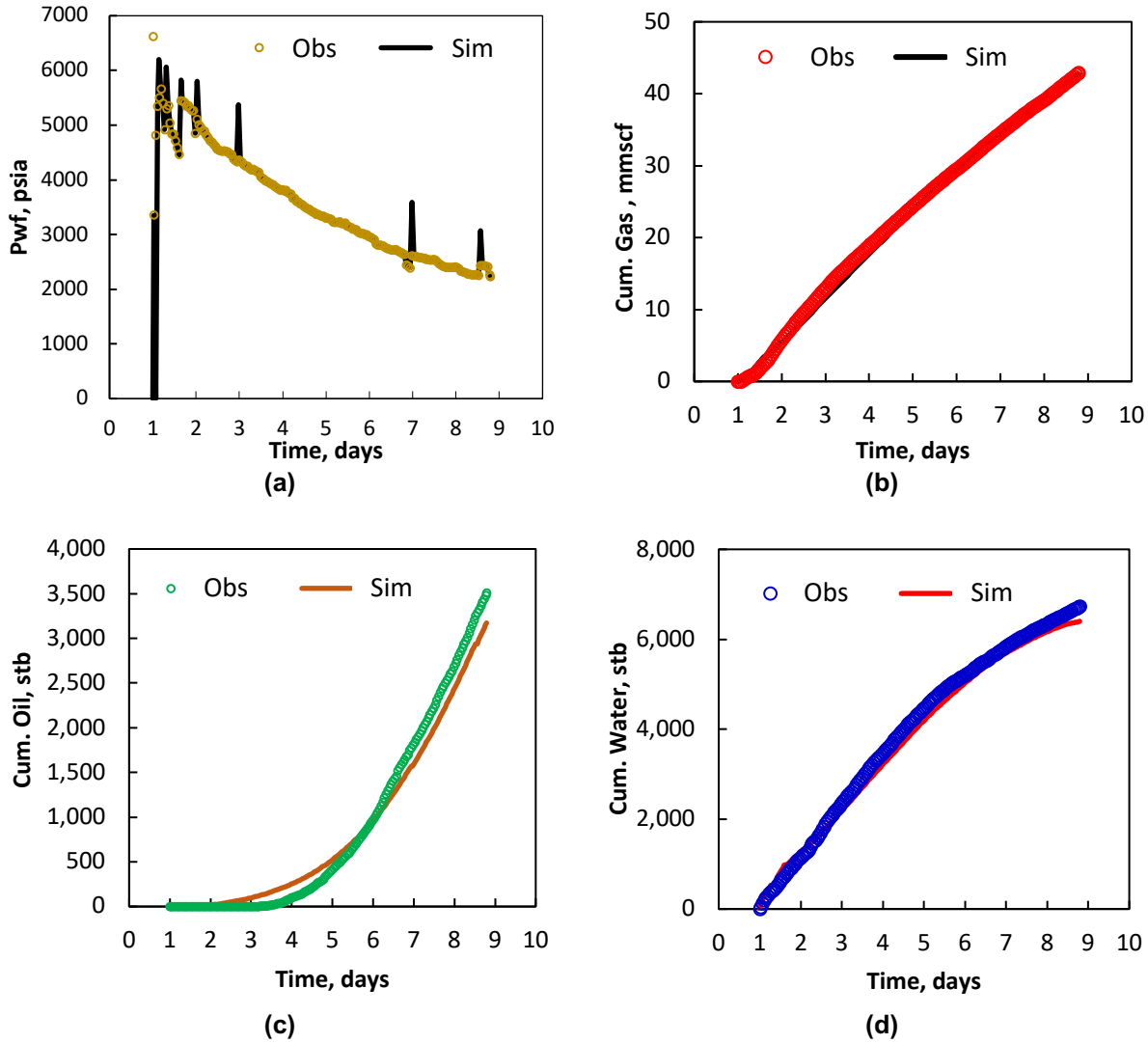

Fig. 16. Final history-match of: (a) flowing bottomhole pressure; (b) cumulative production; (c) cumulative oil production and (d) cumulative water production.

Table 5
Final value of the tuned parameters at the end of history match.

Matching Parameters	Match Value
log10 of Pedrosa coefficient (Propped Fracture)	-5.89
log10 of Pedrosa coefficient (Unpropped Fracture)	-3.86
x_f, ft (Propped fracture)	350
log10 of Permeability (Unpropped Fracture)	4.27
log10 of Permeability (Propped Fracture)	4.75
S_w (Matrix)	0.31
S_{wcrit} (Matrix)	0.13
S_{orw} (Matrix)	0.20
S_{gcrit} (Matrix)	0.19
k_{rwiro}	0.80
k_{rogcg}	0.70
k_{rgcl}	1.00
Ratio of unpropped fracture volume beyond fracture tip to total unpropped volume	0.73
Threshold of Capillary Pressure	150.0
Slope of Capillary Pressure Curve	1.68
N_w (Matrix)	4.00
N_{ow} (Matrix)	4.00
N_{og} (Matrix)	9.35
N_g (Matrix)	6.91
N_w (Fracture)	2.00
N_{ow} (Fracture)	2.00
N_{og} (Fracture)	2.00
N_g (Fracture)	1.98
FORCH Coefficient	1.60
Porosity (Propped Fracture)	0.29
log10 fracture compressibility (Unpropped)	-3.47
log10 fracture compressibility (Propped)	-5.91

Table 6
Final value of the tuned hydraulic fracture parameters at the end of history match.

Matching Parameters	Match Value
HF (half) width (ft)	0.03
HF (total) half-length (ft)	1640
HF (propped) half-length (ft)	350
HF (total) height (ft)	230
HF (propped) height (ft)	175
HF (propped) height – above well (ft)	60
HF (propped) height – below well (ft)	115
HF (propped) permeability (Darcy)	56.2
HF (unpropped) permeability (Darcy)	18.5

Because tuning the relative permeability curves of the matrix and HF constitutes a critical component of the history match effort, the final curves are presented in **Fig. 17**. While the "permeability jail" effect on relative permeability of the matrix is evident, the curves associated with the HF tend towards a straight line shape.

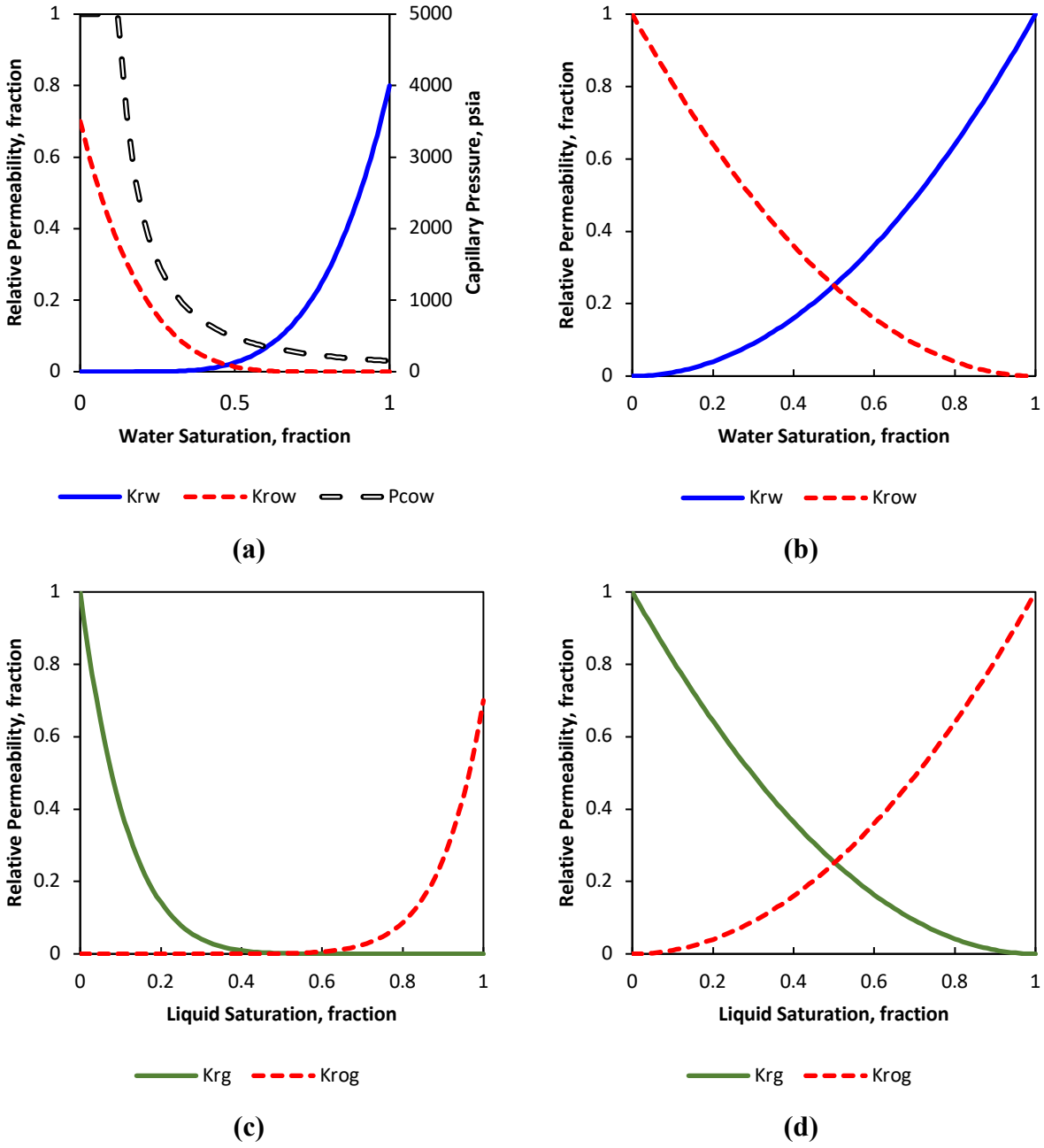

Fig. 17. Tuned two-phase relative permeability curves of oil-water system (a & b) and gas-oil (c & d) system for matrix and HF unpropped region, respectively. The tuned water-oil capillary pressure curve for the matrix is also shown in Fig. 16a.

In order to explore the sensitivity of the objective functions to the primary uncertain parameters, Tornado plots were created for each objective function (for all three phases). For example, **Fig. 18** displays a Tornado plot for the

cumulative water production misfit versus all input parameters (see Table 3). It is evident from Fig. 18 that factor 1 (Pedrosa coefficient of the propped facture) has the largest effect on the water misfit objective. Tornado plots for the other two objective functions (gas, and oil production misfit) were also generated (not shown). The five most important parameters for all these objectives are shown in **Table 7**. Although factor 1 remains consistently the most important parameter for all three different objective functions, the ranking of other factors varies from one objective to another (competing factors). This observation confirms the importance of the application of a multi-objective optimization algorithm, like GA, to tackle a complex problem like flowback production and composition history match.

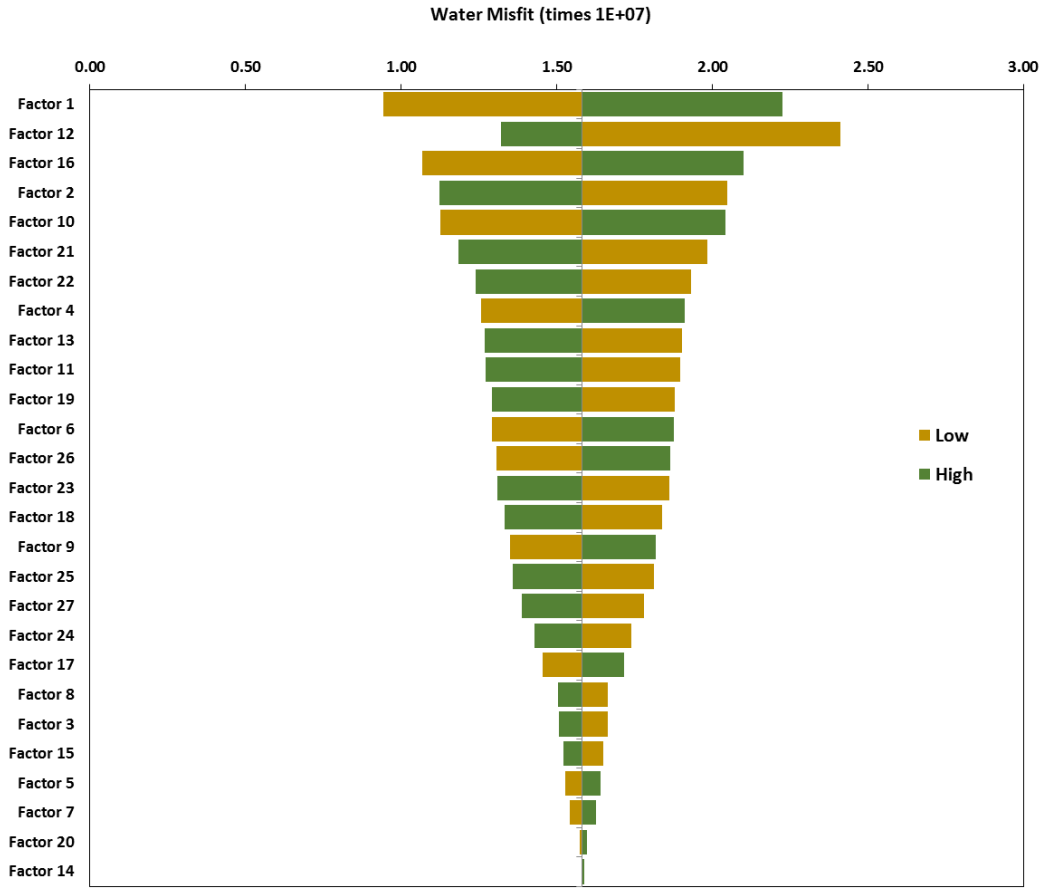

Fig. 18. Tornado diagram of water misfit objective versus all input parameters.

Table 7
Ranking of sensitive input parameters for different objective functions

Ranking	Gas misfit	Oil misfit	Water misfit
1	Factor 1	Factor 1	Factor 1
2	Factor 12	Factor 23	Factor 12
3	Factor 6	Factor 5	Factor 16
4	Factor 10	Factor 2	Factor 2
5	Factor 13	Factor 4	Factor 10

In the following, the use of layer/flowback compositions as a constraint on fracture height is further discussed, along with match uniqueness.

4. Discussion

In this work, an innovative approach for estimating fracture height-growth that integrates a wide range of measured data, is presented. These data were used to generate a geomodel that captures reservoir rock and fluid heterogeneity, which in turn can be used to constrain fracture height-growth estimates.

In order to obtain the history match shown in Fig. 16, a number of reservoir parameters were tuned (Table 5**)**. It is important to note that a unique match is impossible to obtain with this many uncertain parameters. However, the propped fracture volume and gas compositional constraints discussed in Section 2.3 served to reduce the non-uniqueness of the problem. In particular, the gas compositional constraints have significant influence on the history-match. To illustrate this point, a separate automated history-match was performed with a uniform fluid composition, rather than varying fluid composition by layer as in the previous section. The automated history-match run with uniform composition was not able to find a reasonable match for all three phases. In **Table 8**, all solutions with objective functions below a certain threshold are presented. It can be seen that the previous history-match run using varying fluid composition by layer was able to find two matches with objective values below the thresholds. However, the run with uniform composition did not find any. This finding illustrates that inclusion of geologic interval fluid compositions provides an important constraint on history-matching, and importantly, fracture height.

Table 8
Possible solutions of the history match problem with defined threshold values and with two different initial composition settings.

Misfit objective	Composition variation included		Uniform composition
Oil Misfit < 30,000	23,578.45	29,276.63	Not found
Gas Misfit < 5E+12	3.27E+12	1.60E+12	Not found
Water Misfit < 100,000	82,321.55	84,660.45	Not found

The history-match achieved in the "Results" section, and further discussed above, utilized a single realization of the geologic model. However, because multiple realizations (and associated petrophysical properties) were created, it is instructive to investigate the effect of varying reservoir properties on history-match results. Two additional scenarios were therefore run for this purpose: one that had optimistic rock properties (higher permeability and porosity), and another one that had conservative properties (lower permeability and porosity). The automatic history-matching algorithm was able to find two solutions for the conservative scenario within the specified threshold, however, no solutions were found for the optimistic scenario. The solutions of the conservative scenario were comparable to the base scenario above. This indicates that, during flowback, fracture properties have a more significant effect on the history-match results than rock properties. However, this is not true for the optimistic case, where higher rock permeability impacted the model. The solution misfit values of the conservative run are shown in Table 9 and a comparison of the four matches is provided in Table 10. Note that all cases had identical total fracture half-length (as the fracture was fully propagated to the model boundary).

Table 9
Possible solutions of the history match problem with defined threshold values.

Misfit objective	Conservative Case	
Oil Misfit < 30,000	21,990.10	26,888.50
Gas Misfit < 5E+12	2.67E+12	2.63E+12
Water Misfit < 100,000	67,736.48	95,939.5

Table 10
Final value of the tuned hydraulic fracture parameters at the end of history match.

Matching Parameters	Match Value			
	Base Scenario		Conservative Scenario	
	Match 1	Match 2	Match 1	Match 2
HF (half) width (ft)	0.03	0.03	0.03	0.03
HF (total) half-length (ft)	1640	1640	1640	1640
HF (propped) half-length (ft)	350	350	320	320
HF (total) height (ft)	230	215	263	263
HF (propped) height (ft)	175	175	205	205
HF (propped) height – above well (ft)	60	67	73	73

HF (propped) height – below well (ft)	115	108	132	132
HF (propped) permeability (Darcy)	56.2	56.2	75.6	75.6
HF (unpropped) permeability (Darcy)	18.5	18.5	10.4	10.4

Another important point of discussion is that the field example used benefited from the fact that the only hydraulic fracturing stages that were implemented in the well were the heel stages. If all stages were implemented, some of which would have occurred above the compositional marker toward the toe of the well (see Fig. 1), it would have been very difficult to constrain fracture height growth estimates. If the method suggested herein is to be used in cases where the horizontal trajectory is not truly horizontal (deviated, such as the toe-up lateral section illustrated in this work), then flowback of each of the individual stages (and subsequent compositional analysis of the fluids) would be required. Individual stage flowback is not, however, a current practice of the industry.

Lastly, this study utilized gas compositions collected while drilling the well, and hence only sampled reservoir through which the well was drilled. This means that compositional data for reservoir below the well could not be used as a constraint. In this study, it was assumed that the compositions below the well (including within the lower zone) were equal to the deepest measurement point in the well. However, better constraint on fracture height growth would have been obtained if data collected below the well (for example from offset horizontal or vertical wells targeting the lower zone) could have been obtained.

5. Recommendations

The innovative approach described in this work is a low cost alternative and complementary method to microseismic and other methods for fracture height determination. Unlike microseismic, for example, which provides an estimate of created fracture height, the proposed method can be used to estimate fracture height contributing to flow. Microseismic and the proposed method will likely result in different estimates of fracture height, but we believe there is value in the comparison of the results of both methods for use in hydraulic fracture design. Hence, it is recommended that operators implement multiple approaches for fracture height estimation, including the proposed approach, particularly when there are concerns about unwanted fracture height growth and contact with unintended target zones.

The method presented herein is, however, subject to uncertainty. These uncertainties can be reduced by gathering petrophysical and fluid data. To improve data gathering the following is recommended:

1. Frequent sampling of cuttings
2. Calibration of log and core data
3. High resolution production data
4. Bottom hole fluid sample

Lastly, although not undertaken in this study, frac model estimates of fracture height and geometry based on fracture treatment data would serve as an important comparison with the fracture height estimates provided herein. Because of the finely laminated and heterogeneous nature of the geologic zones studied, however, this would require additional data not currently available, such as fine-scale (cm or finer) characterization of mechanical properties. While Ghanizadeh et al. (2015b) did attempt to perform such characterization in portions of the subject reservoir, their evaluations were limited to only a small fraction of the vertical section. In future work, further detailed characterization will be performed and fracture modeling implemented to serve as a comparison with the fracture height estimates obtained in this work.

6. Conclusions

The vertical thickness of a reservoir interval that is in hydraulic communication with a hydraulic fracture cannot be reliably estimated using current methods. This information is of great importance to not only hydraulic fracture design, but to mitigate unwanted fracture growth into non-target zones. In the current work, an innovative method that combines detailed geologic modeling, geochemical fingerprinting of the formation interval containing the well (using gas compositions obtained from drill cuttings), flowback fluid rates and compositions, and stochastic compositional simulation is used to estimate fracture height growth from a horizontal well completed in a tight gas condensate reservoir in Western Canada. The following conclusions can be drawn from the study:

- A compositional marker was identified, above which an average C_1/C_2 ratio of 15.7 occurs versus 2.6 below it;

- The flowback fluid composition (average C_1/C_2 ratio = 7.4) is intermediate between those above and below the compositional marker, suggesting some fracture height growth above the marker;
- Fracture height obtained from history-matching is estimated to be 160 ft (71 ft above the well; 118 ft below it), using compositional data (geologic interval and flowback) as constraints;
- Although a unique fracture height estimate cannot be obtained, due to the large number of uncertain parameters, a reasonable history-match of flowback data can be achieved with the compositional constraints implemented.

Acknowledgements
Chris Clarkson would like to acknowledge Shell, Encana, and Alberta Innovates Technology Futures for support of his Chair position in Unconventional Gas and Light Oil at the University of Calgary, Department of Geoscience. Also, the sponsors of the Tight Oil Consortium, hosted at the University of Calgary, are acknowledged for their support. Partial funding for this study was provided by an NSERC Strategic Project Grant (STPGP) (application no. 463605) to Mayer, Clarkson et al.

Nomenclature

BHP = flowing bottom-hole pressure, psia
Dx = size of the parent simulation grid size in the x direction, ft
Dy = size of the parent simulation grid size in the y direction, ft
Dz = size of the parent simulation grid size in the z direction, ft
CGR = condensate-gas ratio, stb/scf
GDE = gross depositional environments
GR = gamma ray
h = thickness, ft
HF = Hydraulic fracture
k_m = effective permeability of matrix, md
k_{rwiro} = largest value for water relative permeability
k_{rogcg} = *relative permeability to oil at connate gas saturation*
k_{rgcl} = relative permeability to oil at connate liquid saturation
N_F = number of hydraulic fracture stages
N_L = number of utilized logical processors
N_g = Corey exponent for gas relative permeability
N_{og} = Corey exponent for oil phase in oil-gas relative permeability
N_{ow} = Corey exponent for oil phase in oil-water relative permeability
Nx = Number of simulation grids in the x direction
N_w = Corey exponent for water phase in oil-water relative permeability
Ny = Number of simulation grids in the y direction
Nz = Number of simulation grids in the z direction
P_c = critical pressure, psia
p_f = pressure of fracture block, psia
p_i = initial pressure, psia
p_m = pressure of matrix block, psia
P_{thresh} = capillary pressure threshold, psia
q_o = oil flow rate, STB/day
q_w = water flow rate, bbls/day
S_g = gas saturation, fraction
S_{gcrit} = critical gas saturation, fraction
S_o = oil saturation, fraction
S_{orw} = residual oil saturation, fraction
S_w = water saturation, fraction
S_{wcrit} = critical water saturation, fraction
t = time, days
T_c = critical temperature, R
w_i = weighting factor

x_f = hydraulic fracture half-length, ft

Greek Letters

β = capillary pressure power-law exponent
γ = permeability modulus
ϕ_m = matrix total porosity, fraction
ϕ_F = effective porosity of the primary hydraulic fracture, fraction

References

Abbasi, M.A., Ezulike, D.O., Dehghanpour, H., Hawkes, R.V., 2014. A Comparative Study of Flowback Rate and Pressure Transient Behavior in Multifractured Horizontal Wells Completed in Tight Gas and Oil Reservoirs. J. Nat. Gas Sci. Eng. 17, 82-93.

Barree, R.D., Cox, S.A., Gilbert, J.V., and Dobson, M.L., 2005. Closing the Gap: Fracture Half Length from Design, Buildup, and Production Analysis. SPE Production & Facilities 20 (04), 274-285.

Bai, T., et al., 2016. Hydraulic Fracture Modeling Workflow and Toolkits for Well Completion Optimization in Unconventionals. Paper SPE 179137 presented at the SPE Hydraulic Fracturing Technology Conference held in The Woodlands, Texas, USA, 9-11 February.

Beggs, D.H., Brill, J.P., 1973. A study of two-phase flow in inclined pipes. Journal of Petroleum technology, 25(05): 607-617.

Cannon, R.T., and Aminzadeh, F., 2013. Distributed Acoustic Sensing: State of the Art. Paper SPE 163688 presented at the SPE Digital Energy Conference held in The Woodlands, Texas, USA, 5-7 March.

Clarkson C.R., Jensen J.L., Pedersen P.K., Freeman M., 2012. Innovative Methods for Flow Unit and Pore Structure Analysis in a Tight Siltstone and Shale Gas Reservoir. AAPG Bull 96 (2), 355–74.

Clarkson, C.R., Qanbari, F. and Williams-Kovacs, J.D. 2014. Innovative Use of Rate-Transient Analysis Methods to Obtain Hydraulic-Fracture Properties for Low-Permeability Reservoirs Exhibiting Multiphase Flow. The Leading Edge 33 (10): 1108-1122.

Clarkson, C. R., Haghshenas, B., Ghanizadeh, A., Qanbari, F., Williams-Kovacs, J.D., Riazi, N., Debuhr, C., Deglint, H.J. 2016. Nanopores to Megafractures: Current Challenges and Methods for Shale Gas Reservoir and Hydraulic Fracture Characterization. J. Nat. Gas Sci. Eng. 31, 612-657.

Fisher, M.K. and Warpinski, N.R., 2012. Hydraulic-Fracture-Height Growth: Real Data. SPE Production & Operations, 27 (01): 8-19.

Gandossi, L., 2013. An Overview of Hydraulic Fracturing and Other Formation Stimulation Technologies for Shale Gas Production. Scientific and Technical Research series (Report EUR 26347 EN). Joint Research Centre, Institute for Energy and Transport.

Ghaderi, S.M., and Clarkson, C.R. 2016. Estimation of Fracture Height Growth in Layered Tight/Shale Gas Reservoirs using Flowback Gas Rates and Compositions - Part I: Model Development. *In press*, J. Nat. Gas Sci. Eng.

Ghanizadeh, A., Clarkson, C.R., Aquino, S. Ardakani, O.H., Sanei, H., 2015a. Petrophysical and Geomechanical Characteristics of Canadian Tight Oil and Liquid-Rich Gas Reservoirs: I Pore Network and Permeability Characterization. Fuel 153, 664-681.

Ghanizadeh, A., Clarkson, C.R., Aquino, S. Ardakani, O.H., Sanei, H., 2015b. Petrophysical and Geomechanical Characteristics of Canadian Tight Oil and Liquid-Rich Gas Reservoirs: II Geomechanical Property Estimation. Fuel 153, 682-691.

Huo, D., Li, B., and Benson, S.M. 2014. Investigating Aperture-Based Stress-Dependent Permeability and Capillary Pressure in Rock Fractures. Paper SPE 170179, presented at the SPE Annual Technical Conference and Exhibition, held in Amsterdam, The Netherlands, 27-29 October.

Kanfar, M., and Clarkson, C.R. 2016. Reconciling Flowback and Production Data: A Novel History Matching Approach for Liquid Rich Shale Wells. *In press*, J. Nat. Gas Sci. Eng.

Kuppe, F., Haysom, S. and Nevokshonoff, G. 2012. Liquids Rich Unconventional Montney: The Geology and the Forecast. Paper SPE 162824 presented at the SPE Canadian Unconventional Resources Conference held in Calgary, Alberta Canada, 30 October-1 November.

Liu, S., and Valko, P.P., 2015. An Improved Equilibrium-Height Model for Predicting Hydraulic Fracture Height Migration in Multi-Layered Formations. Paper SPE 173335 Presented at SPE Hydraulic Fracturing Technology Conference, The Woodlands, Texas, USA, 3-5 February.

McCain, W.D., 1990. The Properties of Petroleum Fluids. PennWell Books.
Nieto, J., Bercha, R., Chan, J. 2009. Shale Gas Petrophysics – Montney and Muskwa, are they Barnett look-alikes? Canadian Well Logging Society, 30-43.
Pedrosa, O.A., 1986. Pressure Transient Response in Stress-Sensitive Formations. Paper SPE 15115 Presented at SPE California Regional Meeting, Oakland, California, USA, 2-4 April.
Salman, A., Kurtoglu, B., Kazemi, H. 2014. Analysis of Chemical Tracer Flowback in Unconventional Reservoirs. Paper SPE 171656 Presented at SPE/CSUR Unconventional Resources Conference held in Calgary, Alberta, Canada, 30 September – 2 October.
Sookprasong, P.A., Gill, C.C., and Hurt, R.S., 2014. Lessons Learned from DAS and DTS in Multicluster, Multistage Horizontal Well Fracturing: Interpretation of Hydraulic Fracture Initiation and Propagation through Diagnostics. Paper SPE 170512 Presented at IADC/SPE Asia Pacific Drilling Technology Conference held in Bangkok, Thailand, 25-27 August.
van der Baan, M., Eaton, D., Dusseault, M. 2013. Microseismic Monitoring Developments in Hydraulic Fracture Stimulation. Chapter 21 in *Effective and Sustainable Hydraulic Fracturing*, Dr. Rob Jeffrey (Ed.). InTech, DOI: 10.5772/56444. Available from: http://www.intechopen.com/books/effective-and-sustainable-hydraulic-fracturing/microseismic-monitoring-developments-in-hydraulic-fracture-stimulation.
Warpinski, N., 2009. Microseismic Monitoring: Inside and Out. J. Pet. Technol. 61 (11), 80-85.
Warpinski, N., Griffin, L.G., Davis, E. J., and Grant, T., 2006. Improving Hydraulic Fracture Diagnostics by Joint Inversion of Downhole Microseismic and Tiltmeter Data. Paper SPE 102690 presented at the SPE Annual Technical Conference and Exhibition held in San Antonio, Texas, 24-27 September.
Wright, C.A., et al., 1998. Downhole Tiltmeter Fracture Mapping: Finally Measuring Hydraulic Fracture Dimensions. Paper SPE 46194 presented at the SPE Western Regional Meeting held in Bakersfield, California, 10-13 May.
Wheaton, B., Haustveit, K., Deeg, W., Miskimins, J., Barree, R., 2016. A Case Study of Completion Effectiveness in the Eagle Ford Shale Using DAS/DTS Observations and Hydraulic Fracture Modeling. Paper SPE 179149 presented at the SPE Hydraulic Fracturing Technology Conference held in The Woodlands, Texas, USA, 9-11 February.
Williams-Kovacs, J.D., Clarkson, C.R., 2016. A Modified Approach for Modeling Two-Phase Fowback from Multi-fractured Horizontal Shale Gas Wells. In press, J. Nat. Gas Sci. Eng. 30, 127-147.
Yousefzadeh, A., Li, Q., and Aguilera, R., 2015. Microseismic 101: Monitoring and Evaluating Hydraulic Fracturing to Improve Efficiency of Oil and Gas Recovery from Unconventional Reservoirs. Paper SPE 177277 presented at the SPE Latin American and Caribbean Petroleum Engineering Conference held in Quito, Ecuador, 18-20 November.
Zolfaghari, A., Dehghanpour, H., Ghanbari, E., and Bearinger, D. 2016. Fracture Characterization Using Flowback Salt-Concentration Transient. SPE Journal 21 (01): 233-244.